Springer

KSME

Journal of Mechanical Science and Technology 26 (8) (2012) 2413~2423
www.springerlink.com/content/1738-494x
DOI 10.1007/s12206-012-0621-2

# Intelligent fault diagnosis method for marine diesel engines using instantaneous angular speed †

Zhixiong Li[1], Xinping Yan[1,*], Chengqing Yuan[1] and Zhongxiao Peng[2]

[1]*Reliability Engineering Institute, School of Energy and Power Engineering, Key Laboratory of Marine Power Engineering & Technology, Ministry of Transportation, Wuhan University of Technology, Wuhan, 430063, China*
[2]*School of Mechanical and Manufacturing Engineering, University of New South Wales, Sydney, NSW 2052, Australia*

(Manuscript Received October 21, 2010; Revised March 6, 2012; Accepted March 11, 2012)

**Abstract**

The normal operation of marine diesel engines ensures the scheduled completion and efficiency of a trip. Any failures may result in significant economic losses and severe accidents. It is therefore crucial to monitor the engine conditions in a reliable and timely manner in order to prevent the malfunctions of the plants. This work describes and evaluates the development and application of an intelligent diagnostic technique based on the integration of the empirical mode decomposition (EMD), kernel independent component analysis (KICA), Wigner bispectrum and support vector machine (SVM). It is an extension of the previous work on the fault detection for a diesel engine using the instantaneous angular speed (IAS). In this study, in order to solve the underdetermined blind source separation (BSS) problem the combination of EMD and KICA is firstly presented to estimate IAS signals from a single-channel IAS sensor. The KICA is also applied to select distinguished features extracted by Wigner bispectrum. The SVM is then employed for the multi-class recognition of the marine diesel engine faults in an intelligent way. Numerical simulations using a 6-cylinder engine model and real IAS data measured on the ship named "Hangjun 20" are used to evaluate the proposed method. Both the numerical and experimental diagnostic results have shown high efficiency of the proposed diagnostic method. Distinct fault features of the IAS signals have been extracted by the EMD-KICA and Wigner bispectrum, and the fault detection rate of the SVM is beyond 94.0%. Thus, the proposed method is feasible and available for the fault diagnosis of marine diesel engines.

*Keywords*: Intelligent fault diagnosis; Marine diesel engines; Kernel independent component analysis; Wigner bispectrum; Support vector machine; Instantaneous angular speed

## 1. Introduction

Marine power plant is the heart of a vessel. In the last decades, diesel engine has become a priori choice in marine applications, and has been served in more than 99% of large commercial vessels as the prime driver in the propulsion systems [1, 2]. Hence enhancing the reliability and efficiency of marine diesel engines has been a major objective for the engineers in designing, manufacturing and operating the vessels [2]. Any malfunction, fault or failure of the engines off shore may result in significant economic losses and severe accidents as well as possible casualty. Therefore, it is imperative to monitor the machine condition and assess their health states in a timely fashion to prevent breakdowns and ensure the scheduled completion and efficiency of trips.

Up to date various methodologies for condition monitoring and fault diagnosis of marine diesel engines have been put forward [3]. Popular techniques include oil and wear analysis [4], thermodynamic model based method [2], and vibrant analysis [5, 6], etc. However, when using oil analysis techniques transducers are required to be installed inside the cylinder to obtain the acquired information. In practice, the sensors are usually difficult to install and prone to damage. Similar problems also exist in some vibration applications. These disadvantages may result in a declination of their diagnosis reliability and even misdiagnosis. A thermodynamic model has no such drawbacks [2]; however, exact model parameters are often difficult to determine. A simplified approach for diesel engine condition monitoring is the use of instantaneous angular speed (IAS) based on the fact that the IAS contains a lot of information for diesel engine fault diagnosis [5] and the encoder is cheap and easy to install [6, 7]. Hence, since the end of the 1980s attention has been paid to the IAS for diesel engine fault diagnosis [8-13]. Earlier studies have shown that the applications of Fourier transform (FT) for the IAS signal are effective for engine combustion fault detection [8-10]. How-

*Corresponding author. Tel.: +86 2786540357, Fax.: +86 2786549879
E-mail address: lzx___520@163.com
† Recommended by Associate Editor Kyung-Soo Kim
© KSME & Springer 2012

ever, for engines with a high number of cylinders and large moment of inertia, it is very difficult to detect the engine fault using the FT-based approach [6]. Hence, Charles et al. [6, 7] presented a novel polar presentation method to detect the diesel engine faults and proved that the polar presentation was more effective than the fast Fourier transform (FFT). Other advanced techniques, such as the short-time Fourier transform [14], fuzzy system [15], genetic algorithm [16] and artificial neural network [17], etc., can also be found in IAS signal analysis. However, majority of the proposed methods have not considered that a measured IAS signal in a marine diesel engine is in nature a mixture of various excitations due to the high engine inertias, overlapping combustion events and the shocks and vibrations of the valve, crankshaft and piston, etc. [18]. As a result, the measured IAS signal is severely distorted, causing a great difficulty in identifying the patterns of the engine directly from the measured IAS signal using the time-frequency analysis.

Fortunately, the independent component analysis (ICA) is a powerful tool to recover the IAS signal from the original mixture. However, the ICA often suffers from two assumptions in practice [19]. One is the linear mixture assumption, and the other is the underdetermined BSS problem [20], that is, the sensor number is less than the number of sources. Up to date, only limited work has been done to address these two issues simultaneously in the field of mechanic fault diagnosis. To overcome this problem, a combination of empirical mode decomposition (EMD) [20] and kernel ICA (KICA) [21] is put forward to estimate the IAS source from the single channel observation. Herein, the kernel ICA (KICA) proposed by Bach [21] focuses on the nonlinear BSS problems. The advantage of the combination is that it can carry out the nonlinear BSS processing even when the number of sensors is less than the number of independent sources.

On the other hand, the high-order spectrum analysis is proven to be a powerful tool in feature extraction; in particular, the bispectrum can stress the weight of characteristic frequency, identify the phasic information and express nonlinear advantages [22]. However, the classical FT-based bispectrum may not be suitable for the signals with variation of the instantaneous frequency because its stationary kernel of the FT does not match with transient signals [22]. For this reason, the Wigner bispectrum has been proposed owing to the superior resolution of Wigner distribution both in the time and frequency domain [23]. The Wigner bispectrum preserves the essential features of Wigner distribution and hence is capable of dealing with nonlinear signals. Thus, it is sensible to use Wigner distribution to extract comprehensive time-frequency information of transient signals, specifically, the IAS signals in this work.

To diagnose the combustion-related faults of marine diesel engines using the IAS signals, this paper presents an intelligent method based on the integration of EMD-KICA and Wigner bispectrum plus SVMs. Two case studies have been carried out to evaluate and verify the fault detection performance of the proposed method. In case 1 the IAS signals are simulated via a 6-cylinder diesel engine model, while in case 2 the IAS signals are measured on the hydraulic dredger named "Hangjun 20". The diagnostic results of the two cases demonstrate that the proposed diagnostic approach can be used to perform intelligent fault detection for marine diesel engines. Furthermore, to highlight this new approach, comparisons are made against the FastICA, the FFT based bispectrum, and different classifiers, etc.

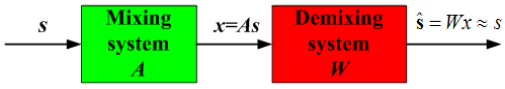


Fig. 1. Illustration of ICA.

## 2. Description of the proposed algorithm

### *2.1 Illustration of kernel ICA*

The concept of ICA is illustrated in Fig. 1. Assume the measured variable data matrix $\mathbf{x} = [x_1\ x_2\ \ldots\ x_n]^T \in R^n$ (where $x_i$ ($i$ = 1, 2 … n) are the same variable measured by the multi-channel sensors). The matrix **x** is the linear combination of $m$ ($m \le n$) unknown independent components (ICs) in matrix $\mathbf{s} = [s_1\ s_2\ \ldots\ s_m]^T \in R^m$. The relationship between **x** and **s** can be expressed as

$$\mathbf{x} = \mathbf{A} \cdot \mathbf{s} \tag{1}$$

where $\mathbf{A} \in R^{n \times m}$ is the mixing matrix. The aim of ICA is to find a transformation matrix $\mathbf{W} \in R^{m \times n}$, $\hat{\mathbf{s}} = \mathbf{W}\mathbf{x} \approx \mathbf{s}$, to make the projection $\hat{\mathbf{s}}$ high order statistically independent (> the second order independent) [24]. Several ICA algorithms, such as FastICA algorithm [20], have been developed to estimate independent components. However, these ICA algorithms are based on a linear model, which has difficulty in dealing with non-linearity cases. To overcome this problem, Bach [21] presented a new method of ICA, named kernel ICA (KICA). His idea regards maximizing independence as minimizing correlation with kernel.

The KICA algorithm can be described briefly as follows. For more details, refer to Bach [21].

Step 1) Center the measured data **x**, choose the appropriate kernel function, and initial the demixing matrix **W**.

Step 2) Whiten the data in the feature space.

Step 3) Compute the centered Gram matrices **K** [21] of the estimated sources.

Step 4) Calculate the maximum eigenvalue $\lambda_F$ of **K**, and do the ICA algorithm to estimate the demixing matrix **W**.

Step 5) Obtain the ICs by $\hat{\mathbf{s}} = \mathbf{W}\mathbf{x}$.

Another promising application of the KICA is the feature reduction. Replace **x** by a feature space **P**, then the output of the KICA is the projection of **P** in a lower dimensionality space, i.e. the reduced feature space **Q** with the redundant

features eliminated.

### 2.2 Underdetermined BSS problem

The ICA technique needs several sensory clues to separate the original source [20]. However, limited by the space of the marine engine room, it is difficult to install multi-channel speed encoders for the diesel engine, hence resulting in the underdetermined BSS problem. To address this issue, an integration of the EMD and KICA is put forward to estimate the IAS source from the single channel sensor observation. The process of the EMD-KICA is described as follows:

(1) Decompose the observation $x(t)$ acquired from the IAS encoder into $n$ intrinsic mode functions (IMFs) using EMD.

(2) Regard the original observation $x(t)$ and the $n$ IMFs as the new multi-channel observations.

(3) Apply the KICA algorithm on the new observations and determine the estimated IAS source from the BSS results.

### 2.3 The flow chart of the proposed diagnostic method

Since the bispectrum analysis can provide more effective fault information than the Fourier transform [22], the Wigner bispectrum is adopted to extract sensitive features of the IAS signal. The Wigner bispectrum extends the standard Wigner distribution in the same way that the bispectrum extends the power spectrum [23].

Given a signal $x(t)$, the Wigner distribution can be expressed as [23]:

$$W_x(t,\omega)=\frac{1}{2\pi}\int_{-\infty}^{+\infty}x^*(t-\tau/2)x(t+\tau/2)e^{-j\tau\omega}d\tau\,. \tag{2}$$

The corresponding Wigner bispectrum is defined by [23]:

$$\begin{aligned}W_x(t,\omega_1,\omega_2)=&\frac{1}{2\pi}\int_{-\infty}^{+\infty}\int_{-\infty}^{+\infty}x^*(t-\alpha\tau_1-\alpha\tau_2)x\\&(t+\beta\tau_1-\alpha\tau_2)x(t-\alpha\tau_1+\beta\tau_2)e^{-j(\omega_1\tau_1+\omega_2\tau_2)}d\tau_1d\tau_2\end{aligned} \tag{3}$$

where $\alpha = 1/3$ and $\beta = 2/3$. Since the energy appears as a spike at the frequency pair $(\omega_1=\omega_2)$ [23], sensitive characteristics of the input data can be extracted efficiently. Moreover, the principal slice [25] of the bispectrum (i.e. the bispectrum diagonal slice) has been used in most applications to capture the distinguished features. Hence, to simplify the calculation, the principal slice of the Wigner bispectrum is applied to the feature extraction of the IAS signal.

Considering that the SVM has strong learning and generalization ability to analyze data and recognize patterns on the basis of limited samples [26], the SVMs are used for the multi-class identification for the fault diagnosis in marine diesel engines in this paper. The proposed diagnostic processes are given as follows:

(1) Estimate $\hat{\mathbf{s}}$ from the raw measured IAS data $\mathbf{x}$ via KICA.


Fig. 2. The schematic diagram of the proposed diagnosis method.

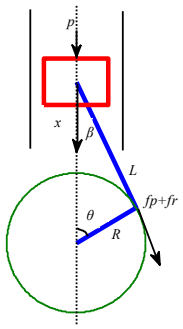


Fig. 3. Dynamics model of a single-cylinder engine.

(2) Calculate the Wigner bispectrum of the estimated IAS waveform in $\hat{\mathbf{s}}$, and extract useful time and frequency information in the Wigner bispectrum to get the original feature space **P**. Then the KICA is employed again to select the distinguished feature to yield a new feature space **Q** (the features in **Q** is less than **P**).

(3) Train the SVMs via **Q** to recognize the fault patterns.

A flow chart of the diagnosis method proposed is illustrated in Fig. 2.

## 3. Case study 1 – Numerical simulation

### 3.1 Data simulation

A simplified dynamic model of a four-stroke single-cylinder diesel engine is shown in Fig. 3, where $p$ is the gas pressure; $f_p$ and $f_r$ are the total tangential forces produced by the gas pressure and the vertical imbalance inertial force, respectively; $\theta$ is the crankshaft angular; and $R$ is the crank radius and $L$ is the length of connecting rod.

The angular speed instantaneous fluctuation ratio (IASFR) is defined as the ratio of the instantaneous angular speed to the average angular speed of a diesel engine, which is given by [5]

$$\varepsilon=\dot{\theta}/\omega\,. \tag{4}$$

The instantaneous angular speed fluctuations of a diesel engine are closely related to the fluctuations of the total power torque acting on the crankshaft. The total power torque is then affected by gas pressure in the cylinder, vertical imbalance inertial force, friction force and engine load, etc.

The torque balance equation can be expressed as [5]

$$I\frac{d^2\theta}{dt^2}=T_X-T_L \tag{5}$$

where $I$ is the inertial moment of the power unit device, $T_X$ is the power torque of the engine, and $T_L$ is the load torque. For

Table 1. The operating parameters of the diesel engine model.

| Cylinder number | 6 | Ignition frequency $f_1$ | 50 Hz |
|---|---|---|---|
| Operating rotating speed $N$ | 1000 rpm | Order of firing | 1-5-3-6-2-4 |
| Operating power $P_0$ | 40 kW | Mass of piston (kg) | 2.88 |
| Basic operating frequency $f_0$ | 8.33 Hz | Mass of connecting rod (kg) | 4.48 |

steady operating condition, the average instantaneous angular speed is a constant, which is expressed as [5]

$$\omega / I = \phi_1(\theta) = \text{constant} . \tag{6}$$

The instantaneous angular speed is defined by [5]:

$$\begin{aligned} \frac{\dot{\theta}}{I} &= \phi_2(\theta) = \int \frac{d^2\theta}{dt^2} = \int \frac{d\dot{\theta}}{d\theta}\frac{d\theta}{dt} \\ &= -\omega \int T_L d\theta + \omega \int Rp(\sin(\theta+\varphi) + \lambda \sin 2(\theta+\varphi)/2) d\theta \\ &\quad + \omega \int 0.5mR^2\omega^2(-\lambda \sin(\theta+\varphi)/2 \\ &\quad + \sin 2(\theta+\varphi) + 3\lambda \sin 3(\theta+\varphi)/2) d\theta \end{aligned} \tag{7}$$

where $\lambda$ is the ratio of crank radius and the length of connecting rod, $m$ is the reciprocating inertial mass and $\varphi$ the initial phase. Since it is difficult to determine $I$ accurately, without knowing the inertial moment $I$, IASFR can be calculated according to Eqs. (6) and (7), which is given by [5]

$$\varepsilon = \frac{\dot{\theta}}{\omega} = \frac{\phi(\theta)_2}{\phi(\theta)_1} . \tag{8}$$

When faults, such as fuel leakage or exhaust valve leakage in a cylinder, influence the gas pressure the IASFR waveforms may be distorted due to the reduction of the torque contribution to the total power torque. Therefore, the IASFR waveform can be used to detect the faults.

A four-stroke and six-cylinder diesel engine (Model 6135G) is selected to simulate the IASFR waveform based on the dynamic model. When the rotational speed of the engine is $N$ rpm, the operating time per engine cycle is $t_0$ = 120/$N$ s, and hence the basic operating frequency $f_0$ of the engine is

$$f_0 = 1/t_0 = N/120 \text{ (Hz)} \tag{9}$$

and the ignition frequency $f_1$ of the engine is

$$f_1 = mf_0 \tag{10}$$

where $m$ denotes the cylinder number.

In the simulation, the operating parameters of the diesel engine are listed in Table 1. The simulation results of the original IASFR waveforms under normal and faulty conditions are shown in Fig. 4. The two faulty conditions include a 50% oil leakage and the oil cutting off in the third cylinder. It can be seen that IASFR waveform varies with the changes in the engine conditions and the physical characteristics of the IASFR are disclosed from the simulation results. Thus, the sensitive characteristic parameters for detecting the faults may be determined from the IASFR waveform.

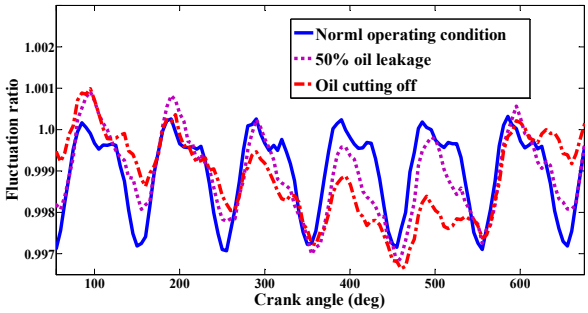


Fig. 4. The original IASFR waveforms of the diesel engine under normal and faulty operating conditions.

### *3.2. Data acquisition using EMD-KICA*

When using an IAS encoder to collect the IASFR signal of the diesel engine in practice, the measured signals may be corrupted by internal and external disturbance signals [18]. For the purpose of simulating this real operating environment of the diesel engine, the following three types of signals are selected to mix with the IASFR waveform to yield the observation **x**. The sinusoid $s_1$ is applied to simulate the low-frequency periodic vibration signal of the gas inlet/outlet valve base; the exponential random signal $s_2$ is used to simulate the shocks caused by the piston knock and the fuel injection pump, etc.; and the random signal $s_3$ is adopted to simulate the cylinder pressure variation. According to Eq. (1), **x** is the linear combination of four independent sources. In the interest of investigating the non-linear case, the addictive noise **n** is imposed to **x**. Thus, Eq. (1) can be rewritten as

$$\mathbf{x_1} = \mathbf{A} \cdot \mathbf{s} + \mathbf{n} . \tag{11}$$

Since the signal-to-noise ratio (SNR) of the speed encoder output is usually greater than 30 dB, the SNR of the addictive noise **n** has been set to be 30 dB in the BSS procedure.

In the BSS procedure, the observation $\mathbf{x_1}$ is firstly decomposed into six IMFs by EMD. Then the six IMFs and $\mathbf{x_1}$ form the new multi-sensory observations as the input of the KICA. The radial basis function (RBF) kernel is adopted for the KICA. Fig. 5 shows the time and frequency spectra of the mixed IASFR under normal condition and Fig. 6 shows the estimated results by EMD-KICA.

Compared with the normal IASFR in Fig. 4, the time spectrum of the estimated normal IASFR in Fig. 6 agrees well with the original one. The large energy peaks locate at $f_1$ and its harmonics and the dominant peak appear at $f_1$. This result is consistent with the outcomes reported in Refs. [5, 10]. Hence, the underdetermined BSS results show that the EMD-KICA

Table 2. The correlation coefficients ($R_f$) using different methods.

| Algorithm | Correlation coefficients ($R_f$) | | | |
|---|---|---|---|---|
| | Estimated $s_1$ | Estimated $s_2$ | Estimated $s_3$ | Estimated IASFR |
| EMD-FastICA | 0.71 | 0.79 | 0.78 | 0.59 |
| EMD-KICA | 0.72 | 0.82 | 0.85 | 0.74 |

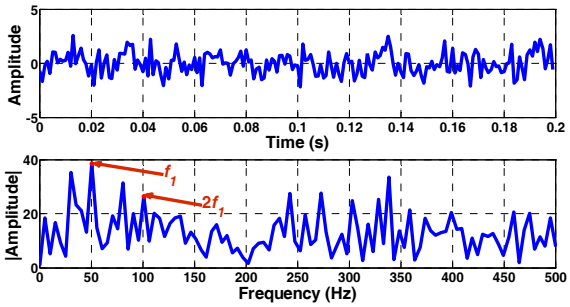


Fig. 5. The time and frequency spectra of the mixed normal IASFR.

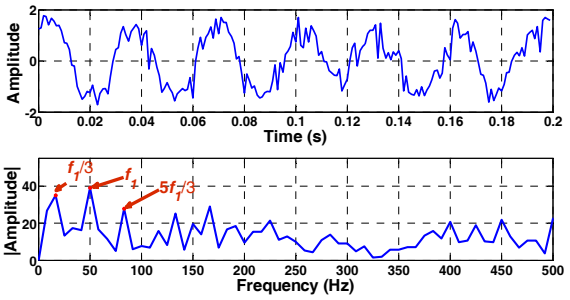


Fig. 6. The time and frequency spectra of the estimated normal IASFR.

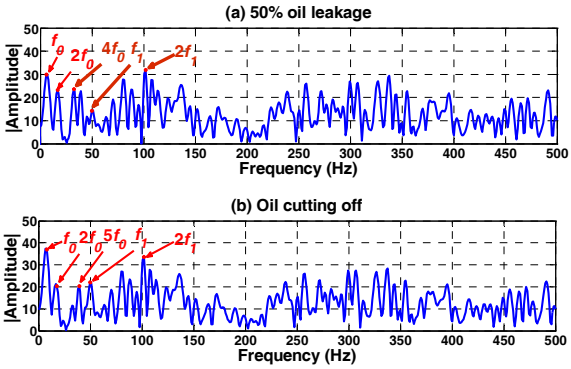


Fig. 7. The frequency spectra of the estimated faulty IASFRs.

method is effective in the IASFR estimation from a single channel observation.

The separation efficiency of EMD-KICA is compared with the EMD-FastICA in this work. The correlation coefficients ($R_f$) between the original sources and the estimated sources are shown in Table 2 for the normal IASFR estimation. The comparison results indicate that the KICA has better correlation coefficients than FastICA, which means the KICA is robust in the estimation of the independent sources in this case.

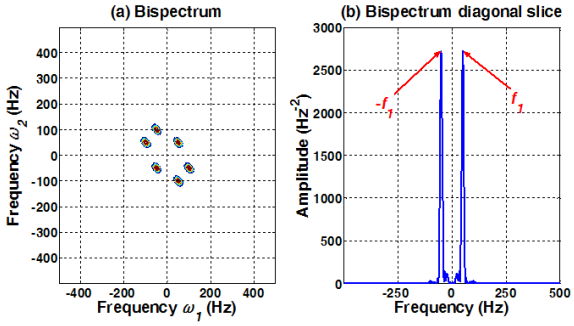


Fig. 8. Results of the normal IASFR via FFT based bispectrum.

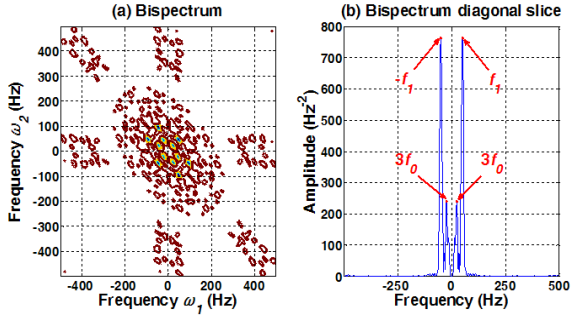


Fig. 9. Results of the 50% oil leakage via FFT based bispectrum.

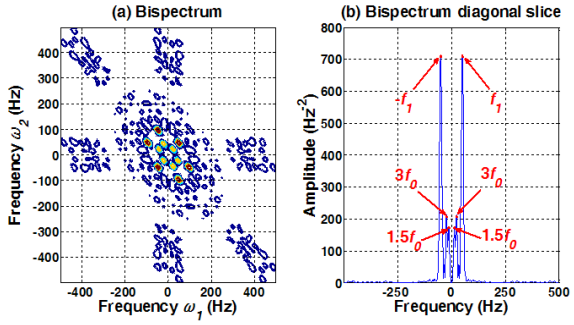


Fig. 10. Results of the oil cutting off via FFT based bispectrum.

Fig. 7 shows the frequency spectra of the estimated IASFRs under the 50% oil leakage and the oil cutting off condition. Compared with Fig. 6, the energy peaks appear at $f_0$ and its harmonics in Fig. 7, which agree with the theoretic analysis well [5, 10]. However, according to Figs. 4-7, it can be seen that it is difficult to determine the engine operation states directly from the time and frequency spectra although there are some differences between the spectra. Hence, the Wigner bispectrum is applied to the feature extraction of the IASFRs.

### *3.3 Feature extraction using Wigner bispectrum*

The Wigner bispectrum analysis is employed to extract sensitive amplitude and phasic features and assess the state of the machine. The performance of the Wigner bispectrum is compared with the classical FFT based bispectrum in the feature extraction. Figs. 8-10 show the bispectrum and the bispectrum diagonal slice of the IASFR signals using the FFT based bis-

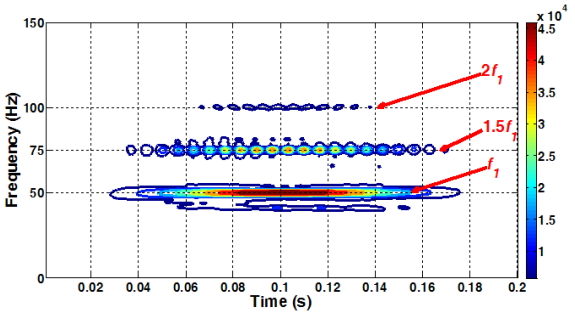


Fig. 11. Results of the normal IASFR via Wigner bispectrum.

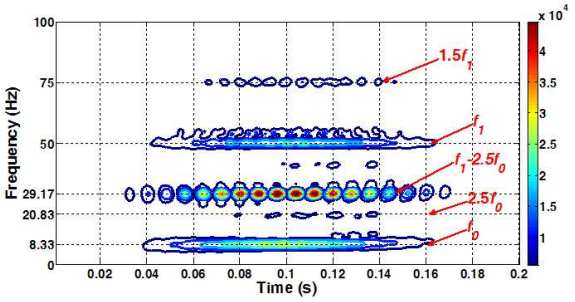


Fig. 12. Results of the 50% oil leakage via Wigner bispectrum.

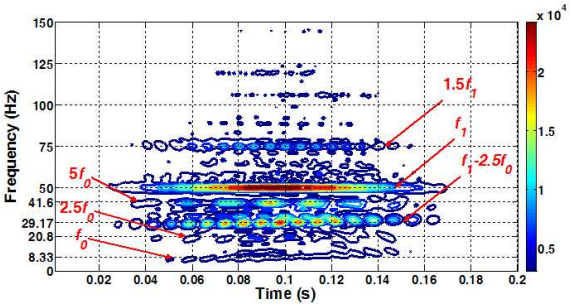


Fig. 13. Results of the oil cutting off via Wigner bispectrum.

pectrum in normal state, 50% oil leakage and oil cutting off in the third cylinder, respectively. Figs. 11-13 show analysis results of the Wigner bispectrum for the three engine operation conditions.

When vibration data from the normal operating engine is analyzed in theory, there are peaks exhibited in the bispectrum at the ignition frequency $f_1$ and $2f_1$, as well as their harmonics. This is because the cylinders work in a balance state. Therefore, the external impacts on the combustion events are small and the ignition explosion makes the main contribution to the IAS fluctuation. Once a failure occurs in the cylinder, the output power of the faulty cylinder decreases greatly, and the other five cylinders need increase their fuel charges to maintain the total engine output power. Thus, the cylinders work in an unbalanced situation, and a coupling effect is arisen between the ignition frequency and basic operating frequency. High peaks would appear at $f_1$ and $f_0$, as well as their harmonics and subtractions and additions, which are caused by the engine working cycle and the coupling effect, etc.

Fig. 8 shows that in normal state high peaks emerge at bi-frequencies (50 Hz, 50 Hz) and (50 Hz, 100 Hz). In the faulty states shown in Figs. 9 and 10, besides $f_1$ high peaks also locate at $f_0$ and its harmonics. The FFT based bispectrum analysis agrees with the theoretical results very well. However, compared with the Wigner bispectrum analysis results in Figs. 11-13, its efficacy is not good enough. More details about the basic operating frequency $f_0$ and its coupling effect with $f_1$ (i.e. $f_1$-$2f_0$, etc.) have been revealed by Wigner bispectrum, and one can be noticed that the coupling effect of $f_1$ and $f_0$ accounts for a large amount of the bispectrum peaks in Figs. 12 and 13. But this coupling information has been completely missed in the FFT based bispectrum. Hence, in contrast to the classical bispectrum, more comprehensive information about sensitive characteristics of the IASFR signals has been presented by the Wigner bispectrum, and the analysis results are superior.

Furthermore, through observing the energy distribution in Figs. 11-13 it can be seen that the amplitudes of the peaks vary with the changes of the working conditions at 8.33 Hz, 29.17 Hz, 50 Hz, 75 Hz and 100 Hz, etc. Hence, the energy information could be used as distinguished features to identify the diesel engine operating conditions. Considering that some distinct features may exist at the high frequency part, a novel method is proposed to search the features as effectively as possible in this work. This approach firstly searches the sum energies in the span of time at frequencies $f_0$, $f_1$ and their harmonics to yield the feature space $\mathbf{P}_{m\times n} = [p\text{m}1, p\text{m}2 \ldots p\text{m}n]$, where subscript $m$ denotes total samples and $n$ is the extracted features. Then the KICA is employed to select the most sensitive features from $n$ features to eliminate the redundancies. Hence the new feature space $\mathbf{Q}_{m\times r} = [q\text{m}1, q\text{m}2 \ldots q\text{m}r]$ $(r < n)$ is obtained, trained and tested as the inputs of a classifier for the pattern recognition.

### *3.4 Pattern recognition by SVM*

Since there may be a certain correlation between the features and the diesel engine states, which may be difficult to express using analytical methods, the SVM is applied to learn the relationship of them. The concept of the kernel trick allows SVM to perform separations even with nonlinear boundaries [27-30]. The kernel type plays a crucial role in the classification process. Since the RBF kernel has been proven more effective than others [27], the RBF kernel is adopted in this article. Moreover, as for the multi-class classification (where one has $k > 2$ classes) using SVMs, the decision method may influence the classification rate. The decision methods based on the one-against-one [29, 30], one-against-all [27] and multi-class support vector (ms-sv) [28] strategies are compared with respect to the classification accuracy here.

In the present work 100 samples for each operating condition (i.e. 300 samples in total) are prepared for the diagnosis procedure, and 40 features for each sample are extracted using Wigner bispectrum. Thus, the original feature space $\mathbf{P}_{300\times 40}$ is obtained. In the feature reduction processing, half of the fea-

Table 3. Classification results using SVM.

| Multi-class strategy | RBF kernel parameter σ | Classification accuracy | | |
|---|---|---|---|---|
| | | $\mathbf{P}_{300\times40}$ | Training | Testing |
| One-against-one | 3 | 47.3% | 96.0% | 93.3% |
| | 8 | 54.7% | 96.0% | 93.3% |
| | 15 | 52.7% | 96.7% | 93.3% |
| One-against-all | 3 | 48.0% | 96.7% | 94.3% |
| | 8 | 56.7% | 96.7% | 94.7% |
| | 15 | 55.3% | 98.0% | 94.7% |
| Mc-sv [25] | 3 | 42.3% | 96.0% | 91.0% |
| | 8 | 55.3% | 96.0% | 90.7% |
| | 15 | 56.0% | 96.0% | 90.7% |

Table 4. Comparison of different diagnosis approaches.

| Feature extraction and reduction method | Classification accuracy (%) | | |
|---|---|---|---|
| | *k*-NN | BP NN | SVM |
| EMD-FastICA-classical bispectrum | 81.7 | 82.3 | 82.0 |
| EMD-FastICA-Wigner bispectrum | 85.3 | 85.7 | 86.3 |
| EMD-KICA-classical bispectrum | 88.3 | 89.0 | 90.7 |
| EMD-KICA-Wigner bispectrum | 93.7 | 93.3 | 94.7 |

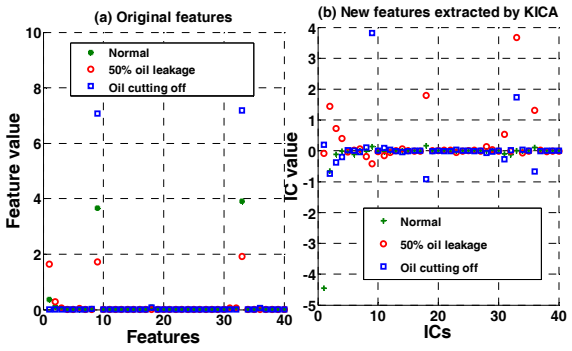


Fig. 14. Feature reduction: (a) original features; (b) new features.

ture space is firstly transformed by the KICA to train the SVM. Then the other half of the features is processed using the same demixing matrix **W** of the training procedure to test the SVM.

A portion of the feature reduction results is shown in Fig. 14. It is noticeable that before the KICA analysis, there are 3 distinguished features (features 1, 9 and 33) related to the three machine states, while this number increased to 8 (features 1, 3, 4, 9, 18, 31, 33 and 36) after the KICA processing. More distinguished features may enhance the diagnosis precision when dealing with a large number of samples. Hence, the eight sensitive features are adopted as the input feature vector for the classifiers in this work.

The comparison of the test results of the SVM classifiers using diverse kernel functions is shown in Table 3. In order to highlight the advantages of the proposed method for the orignial IASFR data processing, the fault diagnostic performance is compared with *k*-nearest neighbor (*k*-NN) and back-propagation neural network (BP NN), as well as different feature extraction and reduction methods. The SVM adopts RBF kernel parameter σ = 15 and one-against-all strategy, *k*-NN chose *k* = 25, and the BP NN used the 8-25-3 structure. The comparison results are listed in Table 4.

Fig. 15. The "Hangjun 20" dredge applied to the experiment tests.

### *3.5 Discussion*

From Table 3, it should be noted that the overall classification rate of the SVM plus KICA feature reduction are dramatically higher than that without KICA reduction. The fault detection rate by SVM without KICA reduction is less than 60%, which indicates that there are a large amount of redundant features in $\mathbf{P}_{300\times40}$ resulting in the unsatisfactory detection rate. In contrast, the average classification rate of the proposed method is greater than 90% in the testing. It is clear that the redundant features in $\mathbf{P}_{300\times40}$ are eliminated efficiently by KICA. Meanwhile, Table 3 shows that the effects of different kernel parameters are small since sensitive input features have been selected by KICA. In addition, in this specific case, the strategy of one-against-all is better than one-against-all and ms-sv with respect to the detection rate.

In Table 4, the fault diagnosis rate has been enhanced by approximate 11% using the KICA when compared with the FastICA. Hence, the KICA is sensitive for the nonlinear IASFR signals due to its kernel trick. Moreover, there is an approximate 4% improvement of the fault identification precision using Wigner bispectrum when compared with the FFT based bispectrum. This is because the Wigner bispectrum can present comprehensive information on the combustion fault during the expansion stroke of the cylinder. It can be also noticed that the classification rates of the *k*-NN, BP NN and SVM are up to 93% or better when using the proposed feature extraction and reduction procedure, and the best performance is 94.7% by the use of the proposed fault diagnosis method.

## 4. Case study 2 – Experimental data processing

The shipboard measurement is carried out in the ship of "Hangjun 20" (see Fig. 15), which is a 300 $m^3$ hydraulic dredger. The fault experiments have been implemented on the diesel power generator "Sweden Volvo Penta TAMD165C".

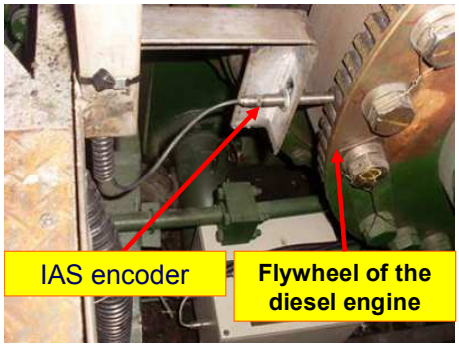


Fig. 16. The IAS sensor arrangement for the dredge diesel generator.

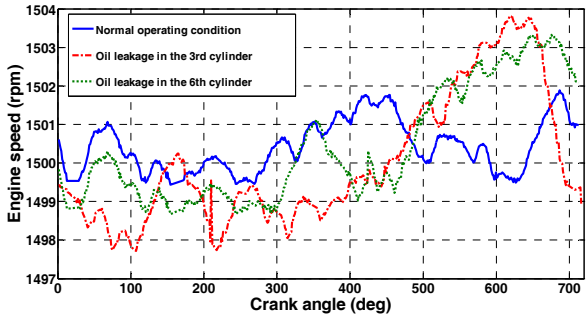


Fig. 17. The estimated IAS signal using EMD-KICA algorithm.

The generator has 6 cylinders and the firing order is 1-5-3-6-2-4. In the experiments, the bolts of the high-pressure oil pipe inject nozzle have been set to loose manually for 3rd cylinder and 6th cylinder, respectively, to simulate the oil leakage faults. The diesel power generator operates for 30 minutes under normal and the two faulty conditions, respectively. The engine rotational speed is 1500 rpm, and hence the basic operating frequency $f_0$ is 12.5 Hz and the ignition frequency $f_1$ is 75 Hz. The speed encoder (see Fig. 16) is located close to the generator flywheel to record the IAS signals.

In this work, the measured raw data is decomposed into 6 IMFs by EMD. The estimated IAS signals of the three operation states of the diesel engine using EMD-KICA are shown in Fig. 17, and their Wigner bispectrum pictures are given in Fig. 18.

It can be seen from Fig. 18(a) that high peaks mainly appear at the coupling frequencies ($f_1$-3.5$f_0$) and ($f_1$-4.5$f_0$). These coupling effects may be arisen by the unbalance inertia-force when the crankshaft is running. During the work cycle, the peak values of the coupling effects change smoothly, however, in the faulty states in Figs. 18(b) and (c), abrupt energy concentrations emerge in short duration. In Fig. 18(b), the sudden energy peaks appear around the time-frequency pairs (400, $f_0$) and [400, ($f_1$-3.5$f_0$)], just after the exhaust stroke of the 3rd cylinder. And in Fig. 18(c), the sudden energy peaks appear around the time-frequency pairs (450, $f_0$) and (450, 2$f_0$), which happen during the expansion stroke and exhaust stroke of the 6th cylinder. It can infer that the combustion faults increase the crankshaft unbalance, and hence the frequency characteris-

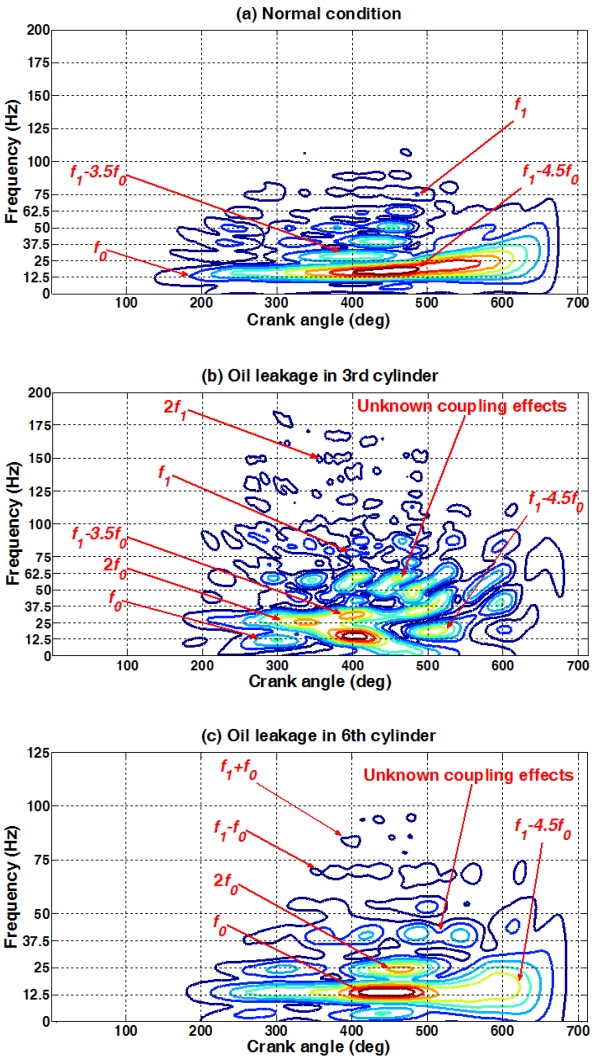


Fig. 18. Analysis results of the estimated real IAS data via Wigner bispectrum: (a) normal data; (b) oil leakage in 3rd cylinder; (c) oil leakage in 6th cylinder.

tics related with the faults behave actively. In addition, a number of small peaks with unknown frequencies are presented in the faulty operations. These characteristics may thus indicate the unknown coupling effects and make a difference between the normal and faulty states of the engine.

One hundred samples for each operating condition (i.e. 300 samples in total) are prepared for the diagnosis procedure, and 40 original features for each sample are extracted using the proposed feature extraction method. Then, half of the features is processed by the KICA to get the new feature space $\mathbf{Q}_{150\times 8}$ for training, followed by the feature reduction of the testing samples using the same demixing matrix $\mathbf{W}$ of the training procedure. In the pattern recognition, the SVM is compared with the $k$-NN and BP NN. The parameters of the classifiers are the same as in the numerical tests in Section 3. The testing result of the SVM using one-against-all strategy is shown in Fig. 19 and the fault identification results are listed in Table 5.

Table 5. The diagnosis results of the experimental data.

| Feature extraction and reduction method | Classification accuracy | | |
|---|---|---|---|
| | *k*-NN | BP NN | SVM |
| Classical bispectrum | 51.3% | 51.7% | 51.7% |
| Wigner bispectrum | 51.7% | 51.7% | 52.7% |
| KICA-classical bispectrum | 88.3% | 88.3% | 89.3% |
| KICA-Wigner bispectrum | 94.3% | 94.3% | 95.3% |

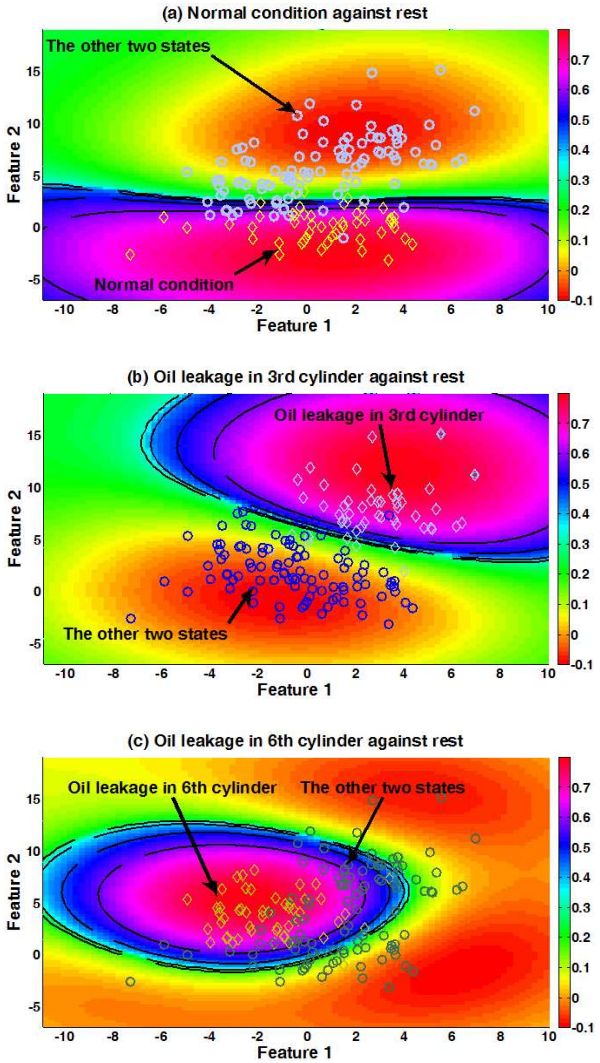


Fig. 19. Training result of the SVM using one-against-all method: (a) normal against rest; (b) 3rd cylinder oil leakage against rest; (c) 6th cylinder oil leakage against rest.

It can be seen from Fig. 19 that the testing data are grouped into three clusters by the SVM. Hence, the SVM could learn the relationship of the input features and the diesel engine states well, which means that the features extracted by the proposed method could effectively represent the characteristics of the IAS data.

It is noticed in Table 5 that the BSS processing and feature reduction via KICA enhance the fault detection rate significantly, the Wigber bispectrum has better performance than the FFT based bispectrum, and the SVM yields the best identification precision among the three classifiers. The experimental results agree well with the numerical simulation results. Thus, the proposed method is feasible and available for the fault diagnosis of marine diesel engines.

## 5. Conclusions

Early fault detection and diagnosis for diesel engines is essential to ensure reliable operation throughout their service lives. The use of the IAS signals is a promising tool for condition monitoring of the diesel engines in practice. Therefore, a new diagnostic method combining the EMD-KICA and Wigner bispectrum plus SVM is proposed to assess the health states of diesel engines. The numerical and experimental analysis results of fault detection and diagnosis show that (a) the non-linear mixed IAS signals can be demixed by the EMD-KICA algorithm from a single channel observation with a small amount of information losing; (b) distinguished features of the IAS signals can be captured by the Wigner bispectrum-KICA method, and hence the fault detection rate can be improved; and (c) the proposed intelligent diagnosis method can detect faults with a high accuracy for the marine diesel engines. Thus, the proposed diagnosis approach in this work may provide practical utilities for marine diesel engines. Further research is to extend the proposed method to the marine gearbox and shaft-line.

## Acknowledgment

The authors thank the National Natural Science Foundation of China (NSFC) for the financial support to the project. This project is sponsored by the State Key Program Grant of NSFC (No. 51139005), the General Grant NSFC (No. 50975213) and the Fundamental Research Funds for the Central Universities (No. 2012-HY-01). The authors are also grateful to the Editors and anonymous reviewers for their constructive advice and comments.

## References

[1] Y. Ishii, A half century with marine diesel engines, *International* Maritime *Technology*, 109 (1) (1997) 33-45.

[2] V. T. Lamaris and D. T. Hountalas, A general purpose diagnostic technique for marine diesel engines – Application on the main propulsion and auxiliary diesel units of a marine vessel, *Energy Conversion and Management*, 51 (4) (2010) 740-753.

[3] J. Son, S. Ahn, J. Bae and M. Ha, Man, Fretting damage prediction of connecting rod of marine diesel engine, *Journal of Mechanical Science and Technology*, 25 (2) (2011) 441-447.

[4] Y. Zhang, J. Mao and Y. Xie, Engine wear monitoring with OLVF, *Tribology Transactions*, 54 (2) (2011) 201-207.

[5] J. Yang, L. Pu, Z. Wang, Y. Zhou and X. Yan, Fault detection in a diesel engine by analysing the instantaneous angular speed, *Mechanical Systems and Signal Processing*, 15 (3) (2001) 549-564.

[6] P. Charles, J. K. Sinha, F. Gu, L. Lidstone and A. D. Ball, Detecting the crankshaft torsional vibration of diesel engines for combustion related diagnosis, *Journal of Sound and Vibration*, 321 (3-5) (2009) 1171-1185.

[7] P. Charles, J. K.Sinha, F. Gu and A. Ball, Application of novel polar representation method for monitoring minor engine condition variations, *Mechanical Systems and Signal Processing*, 24 (3) (2010) 841-843.

[8] G. Rizzoni, Estimate of indicated torque from crankshaft speed fluctuations: a model for dynamics of IC engine, *IEEE Transaction on Vehicular Technology*, 38 (3) (1989) 168-179.

[9] G. F. Mauer and R. J. Watts, Combustion engine performance diagnostics by kinetic energy measurement, *Journal of Engineering for Gas Turbines and Power*, 112 (3) (1990) 301-307.

[10] D. Taraza, N. A. Henein and W. Bryzik, The frequency analysis of the crankshafts speed variation: a reliable tool for diesel engine diagnosis, *Journal of Engineering for Gas Turbines and Power*, 123 (2) (2001) 428-432.

[11] R. Douglas, J. Steel, R. Reuben and T. Fog, On-line power estimation of large diesel engines using acoustic emission and instantaneous crankshaft angular velocity, *International Journal of Engine Research*, 7 (5) (2006) 399-410.

[12] Y. Yu, J. Yang and P. Zhou, Fault diagnosis of a diesel engine by using the analysis of instantaneous angular speed with a flexible model, *International Journal of Vehicle Noise and Vibration*, 7 (4) (2011) 365-385.

[13] Y. Hu, R. Zhou and J. Yang, Research on the fault diagnosis technology of diesel engine based on the instantaneous speed, *Key Engineering Materials*, 413-414 (2009) 547-552.

[14] F. Ponti, Instantaneous engine speed time-frequency analysis for onboard misfire detection and cylinder isolation in a V12 high-performance engine, *Journal of Engineering for Gas Turbines and Power*, 130 (1) (2008) 1-9.

[15] S. Liu, F. Gu and A. Ball, The on-line detection of engine misfire at low speed using multiple feature fusion with fuzzy pattern recognition, *Proceedings of the Institution of Mechanical Engineers, Part D: Journal of Automobile Engineering*, 216 (5) (2002) 391-402.

[16] F. Cruz-Peragón and F. J. Jiménez-Espadafor, A genetic algorithm for determining cylinder pressure in internal combustion engines, *Energy and Fuels*, 21 (5) (2007) 2600-2607.

[17] L. Duan, M. Li and S. Mao, Development of monitoring and fault diagnosing system for ship power plant, *Chongqing Daxue Xuebao*, 32 (1) (2009) 1268-1273.

[18] M. Desbazeille, R. B. Randall, F. Guillet, M. E. Badaoui and C. Hoisnard, Model-based diagnosis of large diesel engines based on angular speed variations of the crankshaft, *Mechanical Systems and Signal Processing*, 24 (5) (2010) 1529-1541.

[19] Y. Jiang, Y. Zhang and J. Wu, Vibration signal processing for gear fault diagnosis based on empirical mode decomposition and nonlinear blind source separation, *Noise and Vibration Worldwide*, 42 (10) (2011) 55-61.

[20] S. Lin, P. Tung and N. E. Huang, Data analysis using a combination of independent component analysis and empirical mode decomposition, *Physical Review E - Statistical, Nonlinear, and Soft Matter Physics*, 79 (6) (2009) 066705.

[21] F. R. Bach and M. Jordan, Kernel independent component analysis, *Journal of Machine Learning Research*, 3 (2003) 1-48.

[22] L. Gelman, I. Petrunin and J. Komoda, The new chirp-Wigner higher order spectra for transient signals with any known nonlinear frequency variation, *Mechanical Systems and Signal Processing*, 24 (2) (2010) 567-571.

[23] N. L. Gerr, Introducing third-order Wigner distribution, *Proceedings of the IEEE*, 76 (3) (1998) 290-292.

[24] X. Tian, X. Zhang, X. Deng and S. Chen, Multiway kernel independent component analysis based on feature samples for batch process monitoring, *Neurocomputing*, 72 (7-9) (2009) 1584-1596.

[25] J. R. Fonollosa and C. L. Nikias, Analysis of finite energy signals using higher order moments and spectra based time-frequency distributions, *Signal Processing*, 36 (3) (1994) 315-328.

[26] Y. Zhang, Enhanced statistical analysis of nonlinear processes using KPCA, KICA and SVM, *Chemical Engineering Science*, 64 (5) (2009) 801-811.

[27] A. Widodo and B. S. Yang, Application of nonlinear feature extraction and support vector machines for fault diagnosis of induction motors, *Expert Systems with Applications*, 33 (1) (2007) 241-250.

[28] J. Weston and C. Watkins, *Multi-class support vector machines*, Egham, UK (1998).

[29] D. Seo, T. Roh and D. Choi, Defect diagnostics of gas turbine engine using hybrid SVM-ANN with module system in off-design condition, *Journal of Mechanical Science and Technology*, 23 (3) (2009) 677-685.

[30] S. Lee, T. Roh and D. Choi, Defect diagnostics of SUAV gas turbine engine using hybrid SVM-artificial neural network method, *Journal of Mechanical Science and Technology*, 23 (2) (2009) 559-568.

**Zhixiong Li** is currently a Ph.D candidate for vehicle application engineering at the School of Energy and Power Engineering of Wuhan University of Technology, China. His current research interests include condition monitoring and intelligent control system.

**Xinping Yan** is currently a professor at the School of Energy and Power Engineering, Wuhan University of Technology, China. He received his Ph.D from Xi'an Jiaotong University, China, in 1997. During Nov. 1997-Jan. 1998, he was invited by the Royal Society as a visiting professor in University of Swansea, UK. He is a member of the editorial committee of *Journal of Condition Monitoring and Diagnostic Engineering Management* and *Proceedings of the Institution of Mechanical Engineers - Part M: Journal of Engineering for the Maritime Environment*. His research interests include condition monitoring, fault diagnosis and application research of tribology.

**Zhongxiao Peng** is currently an associate professor in School of Mechanical and Manufacturing Engineering at The University of New South Wales, Australia. She received her Ph.D in mechanical engineering from the University of Western Australia, Australia, in 2000. During Jan 2008 to May 2011, she was with School of Mechanical Engineering at James Cook University, Australia, as an associate professor. Her research interests include machine condition monitoring and fault diagnosis using wear debris and vibration analysis techniques, and wear analysis of bio-engineering systems.